Capacitive Power Transfer System With a Mixed-Resonant Topology for Constant-Current Multiple-Pickup Applications

Yu-Gang Su, *Member, IEEE*, Shi-Yun Xie, Aiguo Patrick Hu, *Senior Member, IEEE*, Chun-Sen Tang, *Member, IEEE*, Wei Zhou, and Liang Huang

***Abstract*—Capacitive power transfer (CPT) systems based on high-frequency electric field coupling have attracted much attention recently due to their simplicity and low eddy-current losses. This paper proposes a mixed-resonant topology consisted of a Π-*CLC* resonant circuit on the primary side and a T-*CLC* circuit on the secondary side for multiple pickups constant current output applications. The voltage gain, current gain, and zero phase angle frequency at different operating modes of Π-*CLC* and T-*CLC* circuits are analyzed by fundamental frequency approximation, and the conditions leading to a constant output current independent of loads are determined. Based on the analysis, a design method to determine the resonant network parameters is proposed according to the required output current of each pickup. A prototype with three pickups has been designed and built, and both simulation and experimental results have demonstrated that the proposed multiple-pickup CPT system can output a constant current at each operating power pickup against the load variations of itself and others.**

***Index Terms*—Capacitive power transfer (CPT), mixed-resonant topology, multiple pickups, parameter design method.**

I. Introduction

WIRELESS power transfer based on magnetic field has received a lot of attention recently to provide power to a wide variety of applications [1]–[7]. Capacitive power transfer (CPT) employing electric field as the power transfer medium is a new approach for achieving wireless power supplies [8]–[12]. The coupling structure of a typical CPT system consists of two pairs of metal plates, namely the primary and pickup plates [10], [13]–[17]. The pickup plates are coupled with the primary plates via electric filed in between. Two coupling capacitors formed by the two pair plates are usually compensated by a series inductor to increase the power transfer capability.

Recently, due to the design flexibility of the coupling structure and low eddy-current losses in the surrounding metallic objects, CPT technologies have drawn a lot of attention for applications in electric vehicles (EVs) battery charging [8], [9], [18]–[20], consumer electronics, LED lighting [21]–[25], etc. The output of CPT can be either a voltage source or current source, and there is an increasing need for constant current source applications such as battery charging, LED driving, and welding [26]–[28]. And often more than one power pickups are needed to drive multiple loads simultaneously with a single primary CPT circuit. Owing to the variations in capacitive coupling and loads, it is a challenging task to maintain the output of a CPT system to be constant even for a constant voltage source. Liu *et al.* proposed a soft-switching transformer to compensate for the coupling capacitance dynamically when the pickup moves, and designed a primary pad with a matrix structure consisting of multiple subplates to reduce the effect of coupling misalignment. The output voltage can be maintained constant against the positioning and alignment of the pickup on the primary charging pad [29]. Lu *et al.* proposed a double-sided *LCLC*-resonant topology for EV charging applications. The topology can effectively reduce the voltage stress across the power switches of the inverter while maintaining a unity power factor at the ac input [9]. Theodoridis proposed a T-*LCL* resonant topology in the pickup to improve the current ratio between the output current and the displacement current of the coupling structure, so as to extend the load range [30]. These topologies provide high-frequency voltage to drive coupling structures and have zero phase angle (ZPA) between the input voltage and the current, which increases the transfer efficiency. However, there is no work being reported on constant current output applications. And the driving voltages of the coupling structure of the previous systems vary with the load, which works fine with a single pickup CPT system, but cannot be used for multiple loads.

This paper proposes a mixed-resonant topology consisting of a Π-*CLC* resonant circuit on the primary side and a T-*CLC* circuit on the secondary side of a CPT system for multiple pickups constant current output applications, such as for driving LEDs, powering welding machines, and charging batteries

Manuscript received April 28, 2016; revised August 20, 2016 and October 19, 2016; accepted December 5, 2016. Date of publication December 15, 2016; date of current version June 23, 2017. This work was supported in part by the research funds for the National Natural Science Foundation of China under Grants 51477020 and 61573074, and in part by the Chongqing International Science and Technology Cooperation Base Project (CSTC2015GJHZ40001). Recommended for publication by Associate Editor C. T. Rim.

Y.-G. Su is with the Key Laboratory of Dependable Service Computing in Cyber Physical Society (Chongqing University), Ministry of Education, Chongqing 400044, China, and also with the College of Automation, Chongqing University, Chongqing 400044, China (e-mail: su7558@qq.com).

S.-Y. Xie, C.-S. Tang, and W. Zhou are with the College of Automation, Chongqing University, Chongqing 400044, China (e-mail: yunshixie@qq.com; cstang@cqu.edu.cn; zhouwei_cq@163.com).

A. P. Hu and L. Huang are with the Department of Electrical and Computer Engineering, University of Auckland, Auckland 1142, New Zealand (e-mail: a.hu@auckland.ac.nz; lhua571@aucklanduni.ac.nz).

Color versions of one or more of the figures in this paper are available online at http://ieeexplore.ieee.org.

Digital Object Identifier 10.1109/TPEL.2016.2640314

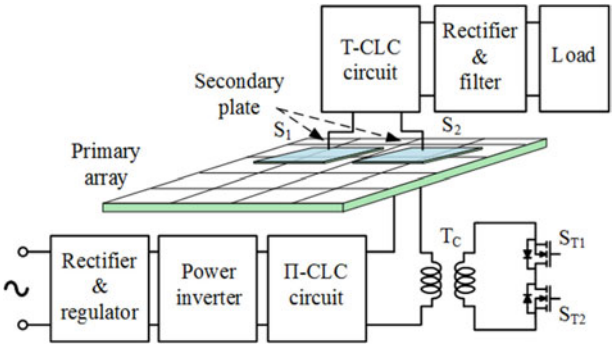

Fig. 1. Block diagram of a CPT system with a mixed-resonant topology.

when a constant current is needed. For the large-area illumination, for example in a traffic tunnel or mine, multiple LED lamps are required to operate at the same time. However, the currents flowing through some LEDs may be affected by the other LEDs when they are switched ON or OFF. The proposed system can keep the output currents constant, which provides an ideal solution to achieve balanced and stable luminance of multiple LEDs. The Π-*CLC* circuit can increase the driving voltage of the coupling structure and maintain it against load variations. Moreover, the T-*CLC* circuit can increase the input current to the output rectifier and keep the output current to be constant against load variations.

The paper is structured as follows: Section II presents the working principle of the CPT system with a mixed-resonant topology. The voltage gain, current gain, and ZPA frequency at different operating modes of the Π-*CLC* and T-*CLC* resonant circuits are analyzed by fundamental frequency approximation in Sections III and IV, respectively. Section V gives a design method considering all the key system parameters according to the required output current of each pickup and the driving voltage of the coupling structure. A prototype is implemented for demonstration and evaluated in Section VI. Section VII concludes the paper.

II. CPT System With a Mixed-Resonant Topology

The block diagram of a CPT system with a mixed-resonant topology is illustrated in Fig. 1. The primary side contains a rectifier and a power regulator to provide a dc current, a high-frequency power inverter to generate an ac current, a Π-*CLC* resonant circuit to increase the driving voltage for the coupling structure, a soft-switched transformer (ST) T_C compensating for the equivalent capacitance of the coupling structure, and a primary array. Noted that the driving voltage for the coupling structure refers to the output voltage of the Π-*CLC* circuit. There can be several pickups on the secondary side, but only one pickup is included in Fig. 1 for simplicity. The pickup side contains two pickup plates, a T-*CLC* resonant circuit to keep the output current constant, a rectifier and filter to provide dc power to the load. The number of pickups is determined by the area of the primary array. The coupling structure is divided into two parts: 1) The primary array consisting of several subplates insulated with each other. The subplates coupling with the pickup plates are selected by controlling relays or triacs. The primary array built in this research is based on the matrix charging platform proposed in [29], where the dynamic tuning control of an ST has been well presented. 2) The pickup plates. The area of each plate is several times larger than that of the subplates. When the pickup plates are placed on the primary array, an alternating electric-field is formed between the selected subplates and the pickup plates. The secondary plate S_1 (S_2) and coupled subplates form a pair of lumped capacitors, whose reactances are canceled out by the compensation transformer.

Fig. 2 shows the circuit diagram of the multiple-pickup CPT system. The Π-*CLC* resonant circuit consists of C_{t1}, C_{t2}, and L_t. The equivalent capacitors of the *j*th pickup coupled with primary array are referred to as $C_{\mathrm{sj}_1}, C_{\mathrm{sj}_2}$. The T-*CLC* circuit is formed by $C_{\mathrm{pj}_1}, C_{\mathrm{pj}_2}$, and L_{pj}. R_j represents the resistance of the equivalent ac load of the *j*th pickup. Parasitic elements of all inductors and capacitors are neglected for the sake of simplicity. The accuracy of the approximation will be validated by the simulations and experiments. Assuming that the distance between the pickup plates and primary array is much smaller than the size of plates, which is acceptable in most CPT system designs [29], [30], the equivalent capacitance is mainly determined by the effective coupled area that would change when a pickup moves in or moves out. The $\mathrm{S_T}$ functions as a variable inductor L_r to compensate for the coupling structure.

III. T-*CLC* Resonant Circuit Analysis

The T-*CLC* resonant circuit used in the pickups is shown in the dashed box on the right side of Fig. 2. The equivalent circuit of the *j*th pickup is plotted in Fig. 3, where pickup voltage is referred to as V_{in}. For simplicity, C_{1T}, C_{2T}, and L_T correspond to C_{pj_1}, C_{pj_2}, and L_{pj}, respectively. According to the relationship among the three reactive components, the resonant circuit can operate at three modes

$$|X_{L_T}| = \begin{cases} |X_{C_{1T}}| & \text{mode one} \\ |X_{C_{1T}}| + |X_{C_{2T}}| & \text{mode two} \\ |X_{C_{2T}}| & \text{mode three} \end{cases}$$

where X_{L_T}, $X_{C_{1T}}$, and $X_{C_{2T}}$ represent the reactances of inductor L_T, capacitor C_{1T}, and C_{2T}, respectively.

The operation of mode one is similar to that of mode three due to the symmetrical structure of the T-*CLC* circuit. Therefore, the following analysis only focuses on the modes one and two

Mode one: $|X_{L_T}| = |X_{C_{1T}}|$.

The input impedance of the resonant circuit is achieved by the circuit theory as follows:

$$Z_{\mathrm{in}} = \frac{1 - \omega_n^2 - \omega_n^2/\lambda_T + j\omega_n/Q_T\left(1-\omega_n^2\right)}{j\omega_n\omega_0 C_{1T}\left(1-\omega_n^2/\lambda_T + j\omega_n/Q_T\right)} \tag{1}$$

where ω, ω_0, ω_n, Q_T, and λ_T are the operating angular frequency, resonant angular frequency, normalized angular frequency, load quality factor, and the ratio of capacitors,

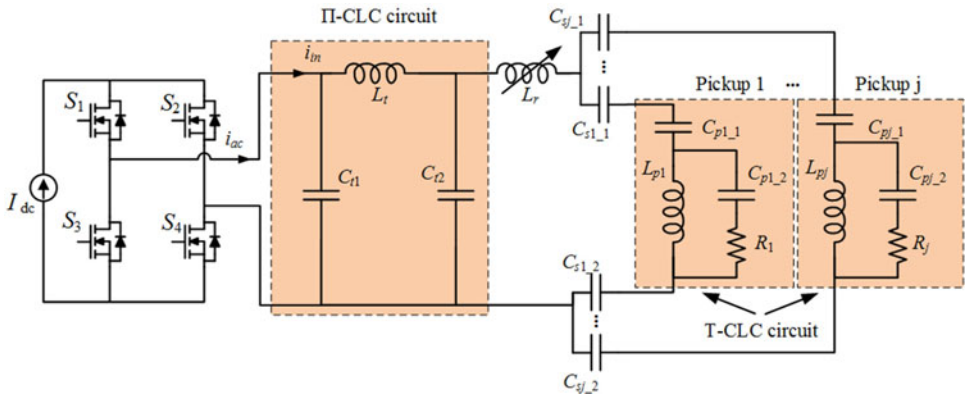

Fig. 2. CPT system with multiple pickups required constant output current.

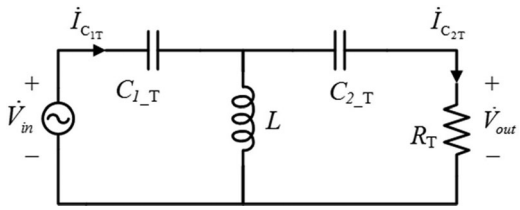

Fig. 3. T-*CLC* resonant network. (a) Contour plot of input angle with respect to $w_{\rm n}$ and $\lambda_{\rm T}$. (b) Contour plot of current gain with respect to $w_{\rm n}$ and $\lambda_{\rm T}$.

respectively, and satisfied

$$\begin{cases} \omega_0 = \sqrt{1/(C_{1T}L_T)} \\ \omega_n = \omega/\omega_0 \\ Q_T = 1/(\omega_0 C_{2T} R_T) \\ \lambda_T = C_{1T}/C_{2T} \end{cases}. \tag{2}$$

The output current of the circuit is given by

$$\dot{I}_{C_{2T}} = \frac{-j\omega_0 C_{2T}\omega_n^3}{1-\omega_n^2-\omega_n^2/\lambda_T + j\omega_n/Q_T(1-\omega_n^2)}\dot{V}_{\rm in}. \tag{3}$$

The current gain of the current flowed through C_{2T} and that passed through C_{1T} can be written as

$$M_i = \left|\frac{\dot{I}_{C_{2T}}}{\dot{I}_{C_{1T}}}\right| = \left|\frac{-\omega_n^2/\lambda_T}{1-\omega_n^2/\lambda_T + j\omega_n/Q_T}\right|. \tag{4}$$

The characteristics of T-*CLC* resonant circuit depend on the combinations of the normalized angular frequency ω_n and the ratio of capacitors λ_T.

a) *Constant-current characteristic*

At the natural oscillation frequency corresponding to $\omega_n = 1$, combining (1), (3), and (4) yields

$$\dot{I}_{C_{2T}} = j\lambda_T\omega_0 C_{2T}\dot{V}_{\rm in} \tag{5}$$

$$M_i = \left|\frac{Q_T}{Q_T(\lambda_T-1)+j\lambda_T}\right| \tag{6}$$

$$Z_{\rm in} = \frac{Q_T}{\lambda_T\omega_0 C_{1T} + j\omega_0 C_{1T}Q_T(1-\lambda_T)}. \tag{7}$$

And when $\lambda_T = 1$, (5)–(7) can be reduced to

$$\dot{I}_{C_{2T}} = \frac{\dot{V}_{\rm in}}{Z_{C_{2T}}},\ M_i = Q_T,\ \ Z_{\rm in} = \frac{Q_T}{\omega_0 C_{1T}}. \tag{8}$$

It can be seen from (5) that the output current $\dot{I}_{C_{2T}}$ is independent of the load R_T at resonance. The output current is boosted Q_T times larger than the input current when the capacitance ratio λ_T equals 1. And the phase angle between the input current and the input voltage is zero, i.e., the resonant circuit operates at the ZPA state achieving a unity power factor. As can be seen from (5), the load current keeps constant as long as $V_{\rm in}$ remains unchanged.

b) *Constant-voltage characteristic*

When the normalized angular frequency satisfies $\omega_n = \sqrt{\lambda_T/(1+\lambda_T)}$, combining (1) and (3) gives

$$\dot{V}_{\rm out} = -\lambda_T\dot{V}_{\rm in} \tag{9}$$

$$Z_{\rm in} = \frac{1}{\omega_0 C_{1T}\left(\lambda_T Q_T + j\sqrt{\lambda_T(1+\lambda_T)}\right)}. \tag{10}$$

As can be seen from (9), the output voltage of the resonant circuit is $\lambda_T(\lambda_T > 1)$ times higher than the input voltage and independent of the load. The minus sign indicates that the output voltage $\dot{V}_{\rm out}$ and input voltage $\dot{V}_{\rm in}$ are opposite in phase. However, the circuit cannot achieve the ZPA condition, necessitating a compensation circuit to cancel out the reactive power which may increase the cost and system complexity.

Mode two: $|X_{L_T}| = |X_{C_{1T}}| + |X_{C_{2T}}|$

Conditions yielding the load-independent output current/voltage are derived with the same analysis.

a) *Constant-current characteristic*

When $\omega_n = \sqrt{\lambda_T/(1+\lambda_T)}$, the combination of (1), (3), and (4) gives (11)–(13), indicating that output current $\dot{I}_{C_{2T}}$ of the circuit is independent of the load R_T

$$\dot{I}_{C_{2T}} = j\omega_n\omega_0 C_{1T}\dot{V}_{\rm in} \tag{11}$$

$$M_i = \frac{Q_T\sqrt{1+\lambda_T}}{Q_T\sqrt{1+\lambda_T}\,(1-\lambda_T) - j\lambda_T} \tag{12}$$

$$Z_{\rm in} = \frac{Q_T\,(1+\lambda_T)}{\lambda_T\omega_0 C_{1T} - j\omega_0 C_{1T}Q_T\sqrt{1+\lambda_T}\,(\lambda_T-1)}. \tag{13}$$

And at the condition of $\lambda_T = 1$, (11)–(13)can be simplified to

$$\dot{I}_{C2T} = \frac{\sqrt{2}j\omega_0 C_{1T} V_{\text{in}}}{2},\ M_i = \sqrt{2}Q_T,\ Z_{\text{in}} = \frac{2Q_T}{\omega_0 C_{1T}}. \quad (14)$$

From (8) and (14), it can be found that both of the output currents of the resonant circuit in modes one and two are independent of the load R_T. But with the same values of circuit components, the current boosting capability of mode two is higher than that of mode one.

b) *Constant-voltage characteristic*

When $\omega_n = \sqrt{\lambda_T/(2+\lambda_T+\lambda_T^2)}$, the output voltage and the input impedance of the circuit can be calculated as

$$\begin{cases} \dot{V}_{\text{out}} = \frac{-\dot{V}_{\text{in}}(1+\lambda_T)}{2} \\ Z_{\text{in}} = \frac{2}{\omega_0 C_{1T}\left[Q_T\left(1+\lambda_T^2\right)+j\sqrt{\lambda_T\left(2+\lambda_T+\lambda_T^2\right)}\right]} \end{cases}. \quad (15)$$

It can be seen from (15) that the output voltage $\dot{V}_{\text{out}}$ of the circuit is also independent of load R_T. However, it cannot work at the ZPA state. Thus, the inverter needs to supply more reactive current, imposing higher current stress on the switching devices.

It is desirable for pickups to include a resonant circuit with improved current boosting capability, so that the load can receive the required output power with only a small current through the coupling structure. Moreover, it is preferred that the resonant circuit works at the ZPA state with a load-independent output current. Based on the analysis in this section, the T-*CLC* resonant circuit operating at mode two can meet these requirements and provide a constant output current regardless of variations of the load.

Since the resonant circuit is a high-order system, there might be another resonance point near ω_0 with a distinctive characteristic, which may significantly affect the circuit performance due to parameter variations. The frequency characteristic of T-*CLC* circuit shown in Fig. 4 is provided to check whether there is a sharp changing resonant point around ω_0. Based on (12) and (13), contour plots of the current gain and the input angle of T-*CLC* circuit at mode two with respect to ω_n and λ_T are plotted in Fig. 4. The dashed circle in the figure means that the circuit operates at the resonant frequency ω_0. Assuming that the quality factor Q_T and the load resistance R_T are 15 and 10 Ω, respectively, the frequency characteristic is analyzed with ω_n and λ_T varying within 2% of the set values at an interval of 4×10^{-5}. The bold line labeled zero in Fig. 4(a) means that another points exist around ω_0 achieving ZPA. And the current gains at these points are slightly smaller than 21 as shown in Fig. 4(b). However, the change from ω_0 to the neighboring points is quite smooth, which indicates no sudden change when the working frequency drifts slightly from ω_0.

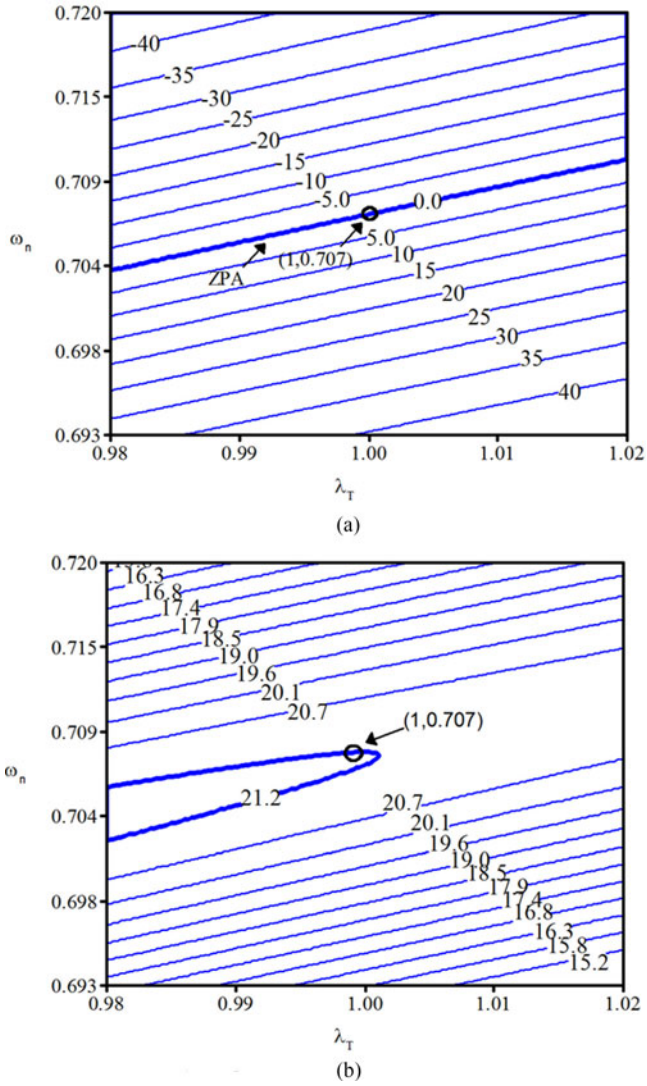

Fig. 4. Current gain sensitivity of T-*CLC* network.

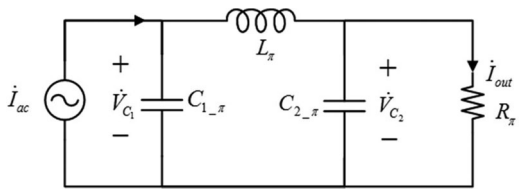

Fig. 5. Π-*CLC* resonant network.

IV. Π-*CLC* Resonant Circuit Analysis

When operating at the designed resonant frequency, the compensation inductor cancels the reactance of the equivalent capacitance of the coupling structure. Moreover, the input impedance of each pickup can be regarded as a pure resistance R_π. Therefore, Fig. 2 can be simplified as Fig. 5, where $C_{1\pi}$, $C_{2\pi}$, L_π correspond to C_{t1}, C_{t2}, L_t, respectively. Similar to T-*CLC* circuit, Π-*CLC* circuit has three working modes. The condition for load-independent voltage/current output can be obtained by the similar analysis applied to T-*CLC* circuit. Meanwhile, it can be found that the current gain is insensitive to the variations of frequency and circuit parameters.

The detailed analysis is omitted due to the page limit. The charateristics of both resonnat circuits are summarized in Table I, where $Q_\pi = \omega_0 C_{2\pi} R_\pi$, $M_{v\_\pi} = V_{C_{2\pi}}/V_{C_{1\pi}}$, $\lambda_\pi = C_{1\pi}/C_{2\pi}$, $\omega_0 = 1/\sqrt{C_{1\pi} L_\pi}$, CC represents constant current output, and CV represents constant voltage output.

TABLE I
PROPERTY OF TWO TYPES OF RESONANT NETWORK

Resonant circuit	Mode	Output characteristics	Conditions	Output	Gain	ZPA
T-*CLC*	One	CC	$\omega_n = 1, \lambda_T = 1$	$I_{C_{2T}} = \omega_0 C_{1T} V_{\rm in}$	$M_i = Q_T$	Y
	Three	CV	$\omega_n = \sqrt{\lambda_T/(1+\lambda_T)}$	$V_{\rm out} = \lambda_T V_{\rm in}$	$M_v = \lambda_T$	N
	Two	CC	$\omega_n = \sqrt{1/(1+\lambda_T)}$	$I_{\rm out} = \sqrt{2}\omega_0 C_{1T} V_{\rm in}/2$	$M_i = \sqrt{2}Q_T$	Y
		CV	$\omega_n = \sqrt{\lambda_T/(2+\lambda_T+\lambda_T^2)}$	$V_{\rm out} = (V_{\rm in}1+\lambda_T)/2$	$M_v = (1+\lambda_T)/2$	N
Π-*CLC*	One	CV	$\omega_n = 1, \lambda_\pi = 1$	$V_{c_{2\pi}} = I_{\rm ac}/\omega_0 C_{2\pi}$	$M_v = Q_\pi$	Y
	Three	CC	$\omega_n = \sqrt{1+\lambda_\pi}$	$I_{\rm out} = I_{\rm ac}/\lambda_\pi$	$M_i = 1/\lambda_\pi$	N
	Two	CV	$\omega_n = 1/\sqrt{1+\lambda_\pi}$	$V_{c_{2\pi}} = \sqrt{2}I_{\rm ac}/\omega_0 C_{2\pi}$	$M_v = Q_\pi/\sqrt{2}$	Y
		CC	$\omega_n = 1, \lambda_\pi = 1$	$I_{\rm out} = I_{\rm ac}/\lambda_\pi$	$M_i = 1/\lambda_\pi$	N

The driving voltage for coupling structure and the operating frequency should be as high as possible to increase the transferred power in per-unit area of the coupling plates. To operate at high frequency, MOSFETs are usually chosen as main switches in the inverter. However, they are desirable to operate at low-voltage for low losses. Thus, there is a contradiction between the requirement of the driving voltage and switches. A resonant circuit that has a voltage boosting capability can relieve this contradiction by placing it between the inverter and the coupling structure. As can be seen from Table I, Π-*CLC* circuit operating at mode one should be selected.

V. RESONANT NETWORK PARAMETER DESIGN

The whole design process is depicted as Fig. 6. The initial driving voltage for the coupling structure V_{d0}, i.e., the voltage across C_{t2}, and the initial operating frequency f_0 are determined empirically. According to the required output current $I_{{\rm out}\_j}(j = 1, 2\ldots)$ and the load resistance R_j in pickups, the components of T-*CLC* circuit can be calculated based on the characteristic equations of mode two working at the CC state as shown in Table I. In practice, a large inductor $L_{\rm pj}$ would lead to excessive winding losses and make the pickups bulky. Therefore, the current boosting capacity of T-*CLC* circuit has an upper limit defined as

$$Q_{T\_j} \le \frac{\omega_0 L_{\max\_j}}{\sqrt{2}R_j} \tag{16}$$

where $L_{\max\_j}$ is dependent on the requirements for the size of the *j*th pickup. If the designed $L_{\rm pj}$ is larger than $L_{\max\_j}$, the design procedure for T-*CLC* circuit in the pickup iterates with an increase Δf as 1% of f_0.

Since voltage gain M_v of Π-*CLC* circuit at the CV state is proportional to R_π as shown in Table I, the output voltage of Π-*CLC* circuit may be slightly higher than the input voltage at heavy load when all pickups are operating simultaneously. To ensure that Π-*CLC* circuit has the voltage boosting capacity at heavy load and the drain–source voltage of MOSFETs are under the maximum ratings, the following equations should be satisfied:

$$M_{v\_\pi} = Q_{\pi-h} = \omega_0 C_{t2} Z_h = \frac{\omega_0 C_{t2}}{\sum_{j=1}^{j={\rm num}} 1/\,Z_{T\_j}} \ge \frac{V_d}{V_{\rm DS}} \tag{17}$$

where Z_h, $Q_{\pi-h}$, *num*, Z_{T_j}, and $V_{\rm DS}$ represent the equivalent impedances of all the pickups, the quality factor of Π-*CLC* circuit at heavy load, the number of pickups, impedance of the $j_{\rm th}$ pickup, and the rated voltage of MOSFETs, respectively. When the voltage gain M_{v_π} is obtained, C_{t2} can be calculated from (17). At light-load where only one pickup is working, if the voltage gain of Π-*CLC* circuit is excessively high, the fundamental component of $\dot{\mathbf{V}}_{\rm Ct1}$ would be much smaller than the high-order harmonic that can pass through the Π-*CLC* circuit, causing the output voltage V_d of Π-*CLC* circuit not to be stabilized at the set point. This means the voltage gain has an upper limit. Surprisingly, the high-order harmonic plays a leading role in driving voltage for the coupling structure. This requires that the amplitude of $v_{\rm Ct1}$ cannot be lower than that of the high-order harmonic, which can be expressed as

$$M_{v\_\pi} = Q_{\pi-l} \le n10^{20/\,\delta} \tag{18}$$

where $Q_{\pi-l}$ is the quality factor of Π-*CLC* circuit at light load. *n* is the order of the high-order harmonic obtained from the bode diagram. Thus, the voltage gain of Π-*CLC* circuit M_{v_π} ranges from $V_d/V_{\rm DS}$ to $n10^{20/\delta}$. If (18) is unsatisfied, the design of T-*CLC* circuits repeats in turn with an increase of $I_{{\rm out}\_j}$ until it is satisfied. The increase part is represented as ΔI that is selected as 10% of $I_{{\rm out}\_j}$. The components of Π-*CLC* circuit are determined by their characteristic equations of mode one operating at the CV state as shown in Table I. From the Fourier analysis, the dc current $I_{\rm dc}$ can be expressed as

$$I_{\rm dc} = \frac{\pi\sqrt{2}}{4} I_{{\rm ac}\_\pi}. \tag{19}$$

In order to guarantee the system safety, the voltage across C_{t1} in Fig. 2 is required to be monitored in real time. If $v_{\rm Ct1}$ is lower than a certain value $V_{\min}$, which indicates all pickups move out, the system would operate at no-load state. If $v_{\rm Ct1}$ is higher than a threshold voltage $V_{\max}$, which means there is a short circuit between the primary subplates, the system would malfunction. The input voltage is reduced when each of these

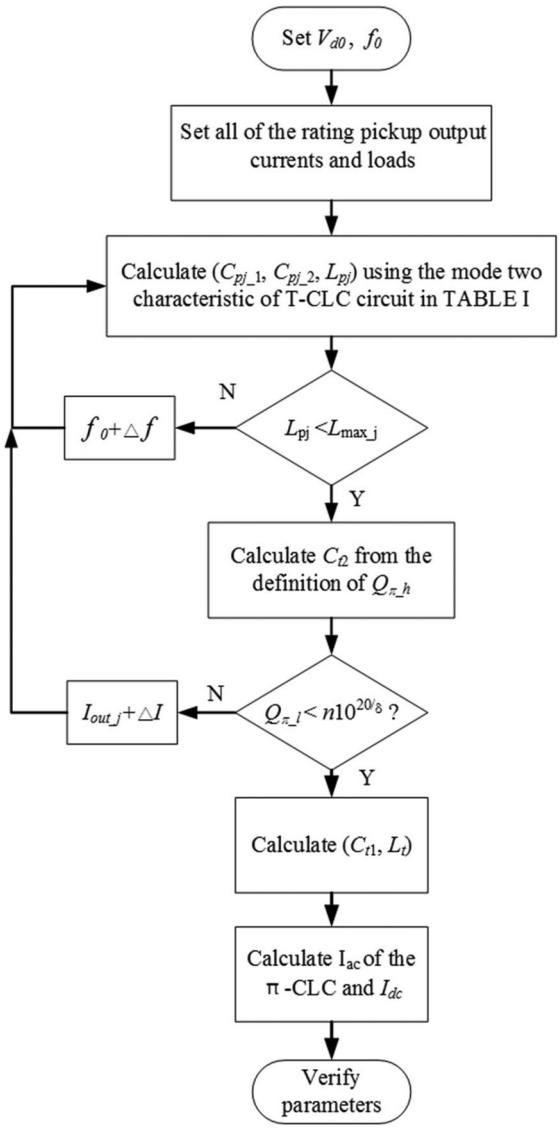

Fig. 6. Design procedure for determining resonant network parameters.

TABLE II
PARAMETERS OF SIMULATION AND EXPERIMENT

Variable	Value	Variable	Value	Variable	Value
R_1/Ω	10	R_2/Ω	15	R_3/Ω	20
$I_{\text{out\_1}}$/A	2	$I_{\text{out\_2}}$/A	2.5	$I_{\text{out\_3}}$/A	3
C_{1-p1}/nF	1.27	C_{2-p1}/nF	1.27	L_{p1}/μH	79.5
C_{1-p2}/nF	1.59	C_{2-p2}/nF	1.59	L_{p2}/μH	63.6
C_{1-p3}/nF	1.9	C_{2-p3}/nF	1.9	L_{p3}/μH	53
C_{t1}/nF	0.79	C_{t2}/nF	0.79	L_t/μH	126.8
V_d/V	500	f/ kHz	500	I_{dc}/A	1.39

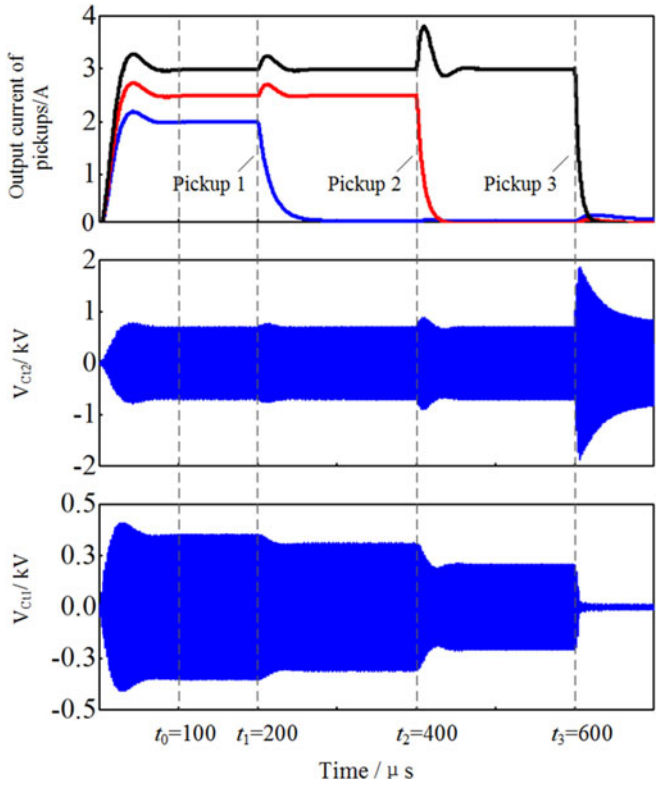

Fig. 7. Simulated waveforms of three pickups operation.

situations occurs. The values of $V_{\min}$ and $V_{\max}$ are determined by the practical requirements.

VI. SIMULATION AND EXPERIMENTAL RESULTS

A. Simulation Results

A CPT system model with three pickups was simulated in MATLAB. Circuit parameters are listed in Table II. Simulated results of three pickups removed in sequence are shown in Fig. 7. During $t_0 - t_1$ period when system is operating at the steady state, rms values of the input currents of the three pickups are 78, 195.6, 355 mA. Corresponding current boosting ratios of T-*CLC* circuits are 25.5, 12.8, 8.4, matching well with theoretical results. Pickups 1, 2, and 3 are moved out at t_1, t_2, t_3, respectively. It can be seen that the output current of operating pickups remains constant despite the changes from other pickups. The voltage across C_{t2} maintains at rated value 500 V. After pickup 1 is moved out, the output current of pickup 2 varies within 8%. And the output current of pickup 3 changes within 6% and 30% after pickups 1 and 2 are moved out, respectively. This happens because the output voltage of Π-*CLC* circuit takes several switching cycles to restore to the original value when the pickups are moved out. All pickups are moved out at t_3. Voltage across C_{t2} is far beyond 500 V. Therefore, the input voltage should be reduced in order to minimize system losses at this moment. Fig. 8 shows simulated waveforms at light-load with pickup 3. The resistive load of pickup 3 changes from 20 to 15 Ω at t_1, and increases to 25 Ω at t_2. It can be seen that the output current of pickup 3 changes within the range of 8% after the load changes. The output current maintains at rated value of 3 A essentially. The output voltage of Π-*CLC* circuit maintains at 500 V.

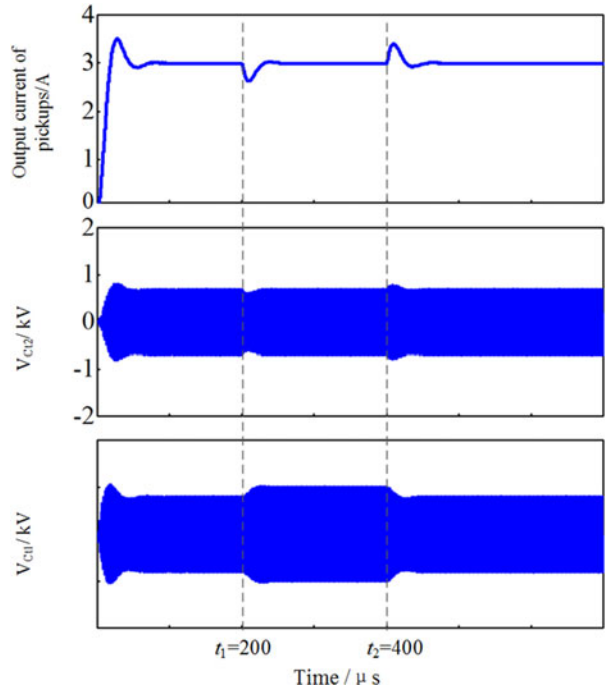

Fig. 8. Single pickup operation.

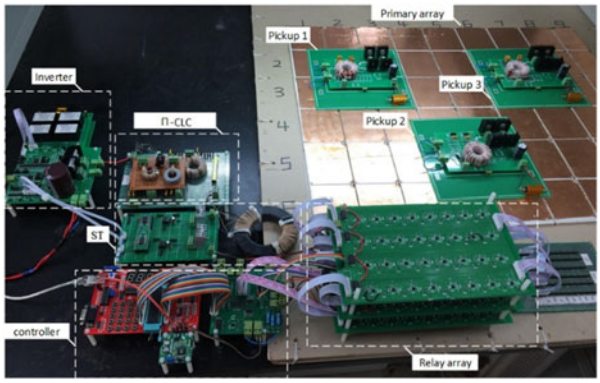

Fig. 9. Prototype CPT system with mixed-resonant topology for multiple-pickup application.

B. Experimental Results

To validate the proposed method and evaluate the performance, a prototype with three pickups has been built as shown in Fig. 9, which has the same parameter values as that of simulation model listed in Table II. The pickup plates of pickups were made up of two copper plates with the dimensions of 100 mm × 200 mm × 35 μm, which were printed on the printed circuit boards. A total of 54 copper plates with the dimensions of 90 mm × 90 mm × 0.1 mm were used as primary subplates. They were all of a rectangular shape. The vertical distance between the coupled primary and pickup plates was 0.2 mm, and insulated with each other by antistatic plastics, yielding an equivalent dielectric constant of $\varepsilon_r = 3.7$. The equivalent capacitance formed by the primary and pickup plates under the fully aligned condition was about 1.56 nF. Through detecting the positions of the secondary plates coupled with the primary subplates and driving the corresponding subplates, the power pickups may obtain a better flexibility in movement [29]. Switching devices of the full-bridge inverter were STP10NM50 MOSFETs. Capacitors used were all of the silvered-mica type so as to ensure the reliability. To obtain a high efficiency and ensure that the voltage stress on the coupling structure is less than the breakdown voltage of the dielectric materials, the terminal voltage was chosen to be 500 V empirically. The inductors used were wound on iron-powder cores from MICROMETALS. Considering the tradeoff between magnetic losses and the physical size of the coupling plates, the operating frequency was chosen to be 500 kHz.

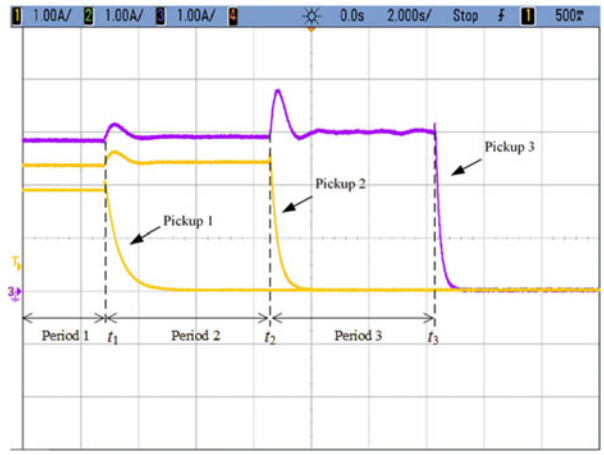

Fig. 10. Output current waveforms of pickups.

The selection of subplates was realized by controlling the relays. The on/off states of the relays depend on the positions of the secondary plates. The detection method for determining the position of the secondary plates is based on a matrix switching method presented in [29]. The principle of locating the secondary plates is to utilize the fact that the coupling condition between a secondary plate and two adjacent primary subplates can be reflected by the current flowing through the primary subplates driven by an ac voltage. Therefore, the subplates coupled with the secondary plates can be determined by driving all of the two adjacent subplates in turn. Then, these subplates are connected to the primary resonant circuit by the corresponding relays. S_T with a turn ration of 1:1 was used as the variable inductor L_r. Magnetizing inductance of the primary winding of the transformer was about 350 μH.

The output currents waveforms of the pickups in the prototype are shown as Fig. 10. Pickups 1, 2, and 3 are moved out at t_1, t_2, and t_3, respectively. It can be seen that the output currents of operating pickup remain constant basically when other pickups move out. The output current of operating pickups spent more time than simulated results to restore to the stable value, because the filtering capacitors were larger than those used in simulation. The steady-state values of the output currents of pickups, driving voltage for coupling structure, and system efficiency in different periods are listed in Table III. As can be seen that the output currents of pickups 2 and 3 increase slightly when pickup 1 moves out, and the system efficiency improves simultaneously because of the reduced losses in MOSFETs and equivalent series resistance losses in Π-*CLC* circuit at light-load. When three pickups operate at the rated state, the prototype can achieve

TABLE III
OUTPUT CURRENTS AND EFFICIENCY OF EXPERIMENT SYSTEM

	Pickup 1 I_{out}/A	Pickup 2 I_{out}/A	Pickup 3 I_{out}/A	Driving voltage /V	η
Period 1	1.83	2.21	2.76	478	79%
Period 2	–	2.31	2.84	489	84%
Period 3	–	–	2.94	496	91%

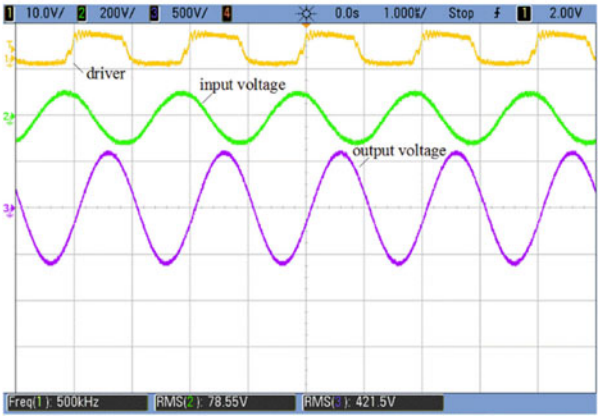

Fig. 11. Π-*CLC* resonant network experiment waveforms.

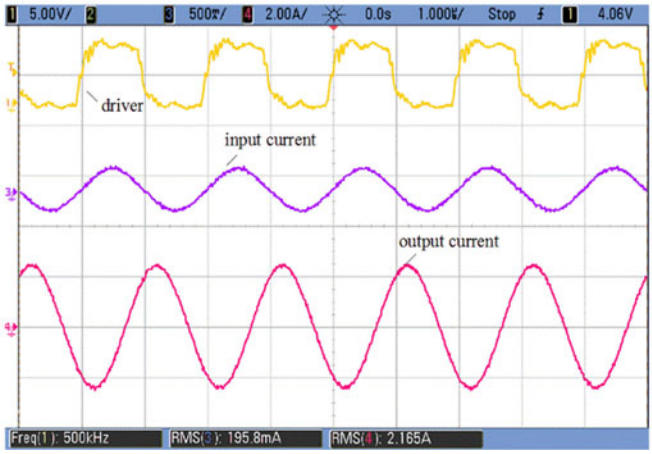

Fig. 12. T-*CLC* network waveforms.

an efficiency of 79% at 260 W. Because of the errors between the selected components in practice and the calculated values, there is a small deviation between the designed output current and the theoretical value. Even though T-*CLC* circuit may not completely exclude the use of regulation circuits, it provides a relatively small load current variation. Note that the power transfer capacity, coupling distance, and physical size of the coupling plates are just some experimental setup parameters. The proposed system may be used for contactless power transfer applications with essentially zero coupling distance to avoid direct electrical contact [8], [15], [18], [22], [31]. There are many methods that can be used to improve the power transfer distance and capacity [9], [32]–[34].

To validate the output boosting capability of Π-*CLC* and T-*CLC* circuit, a light-load operation with only one load R_2 was performed. Fig. 11 shows the voltage waveforms of Π-*CLC* circuit. It can be seen that the output voltage V_{Ct2} of Π-*CLC* circuit is about 5.35 times as large as the input voltage V_{Ct1}, slightly lower than calculated value 6.32. Fig. 12 shows the current waveforms of T-*CLC* circuit. The output current I_{C2} of T-*CLC* is about 11.10 times higher than input current I_{Cl1}, slightly less than theoretical value 12.8. It is caused by the equivalent series resistance of the ST and the inductor of Π-*CLC* circuit.

VII. CONCLUSION

This paper presented a mixed-resonant topology-based CPT system with multiple secondary pickups for constant current output applications. A Π-*CLC* resonant circuit has been proposed to maintain the driving voltage of the coupling structure independent of coupling and load variations; and the T-*CLC* circuit has been proposed to provide a constant current at the output. The full characteristics of the resonant networks including the voltage gain, current gain, and ZPA frequency of the Π-*CLC* and T-*CLC* circuit operating at different modes have been analyzed, and a design method for determining the network parameters has been proposed. A prototype with three pickups has been built to validate the characteristics of the proposed topology, and simulation and experimental results have demonstrated that the output current of each operating pickup can be maintained to be constant against large load variations, even when other pickups are removed.

REFERENCES

[1] S. Y. Choi, J. Huh, W. Y. Lee, and C. T. Rim, "Asymmetric coil sets for wireless stationary EV chargers with large lateral tolerance by dominant field analysis," *IEEE Trans. Power Electron.*, vol. 29, no. 12, pp. 6406–6420, Dec. 2014.
[2] W. X. Zhong, C. Zhang, X. Liu, and S. Y. R. Hui, "A methodology for making a three-coil wireless power transfer system more energy efficient than a two-coil counterpart for extended transfer distance," *IEEE Trans. Power Electron.*, vol. 30, no. 2, pp. 933–942, Feb. 2015.
[3] Z. Wei, W. Siu-Chung, C. K. Tse, and C. Qianhong, "Design for efficiency optimization and voltage controllability of S-S compensated inductive power transfer systems," *IEEE Trans. Power Electron.*, vol. 29, no. 1, pp. 191–200, Jan. 2014.
[4] A. Kamineni, G. A. Covic, and J. T. Boys, "Analysis of coplanar intermediate coil structures in inductive power transfer systems," *IEEE Trans. Power Electron.*, vol. 30, no. 11, pp. 6141–6154, Nov. 2015.
[5] K. Lee, Z. Pantic, and S. M. Lukic, "Reflexive field containment in dynamic inductive power transfer systems," *IEEE Trans. Power Electron.*, vol. 29, no. 9, pp. 4592–4602, Sep. 2014.
[6] W. Wei, Y. Kawahara, N. Kobayashi, and T. Asami, "Characteristic analysis of double spiral resonator for wireless power transmission," *IEEE Trans. Antennas Propag.*, vol. 62, no. 1, pp. 411–419, Jan. 2014.
[7] Y. Su, H. Zhang, Z. Wangi, A. Patrick Hu, L. Chen, and Y. Sun, "Steady-state load identification method of inductive power transfer system based on switching capacitors," *IEEE Trans. Power Electron.*, vol. 30, no. 11, pp. 6349–6355, Nov. 2015.
[8] J. Dai and D. C. Ludois, "Single active switch power electronics for kilowatt scale capacitive power transfer," *IEEE J. Emerg. Select. Topics Power Electron.*, vol. 3, no. 1, pp. 315–323, Mar. 2015.
[9] F. Lu, H. Zhang, H. Hofmann, and C. Mi, "A double-sided LCLC compensated capacitive power transfer system for electric vehicle charging," *IEEE Trans. Power Electron.*, vol. 30, no. 11, pp. 6011–6014, Nov. 2015.
[10] L. Huang and A. P. Hu, "Defining the mutual coupling of capacitive power transfer for wireless power transfer," *Electron. Let.*, vol. 51, no. 22, pp. 1806–1807, Oct. 2015.
[11] K. H. Yi, "6.78 MHz capacitive coupling wireless power transfer system," *J. Power Electron.*, vol. 15, no. 4, pp. 987–993, Jul. 2015.
[12] Y. Su, W. Zhou, A. P. Hu, C. Tang, and R. Hua, "A shared channel design for the power and signal transfers of electric-field coupled power transfer systems," *J. Power Electron.*, vol. 16, no. 2, pp. 805–814, Mar. 2016.
[13] L. Chao, A. P. Hu, G. A. Covic, and N. C. Nair, "Comparative study of CCPT systems with two different inductor tuning positions," *IEEE Trans. Power Electron.*, vol. 27, no. 1, pp. 294–306, Jan. 2012.

[14] C. Liu, A. P. Hu, and N. K. C. Nair, "Modelling and analysis of a capacitively coupled contactless power transfer system," *IET Power Electron.*, vol. 4, no. 7, pp. 808–815, Jan. 2011.
[15] D. Jiejian and D. C. Ludois, "A survey of wireless power transfer and a critical comparison of inductive and capacitive coupling for small gap applications," *IEEE Trans. Power Electron.*, vol. 30, no. 11, pp. 6017–6029, Nov. 2015.
[16] T. Ohira, "Extended k-Q product formulas for capacitive- and inductive-coupling wireless power transfer schemes," *IEICE Electron. Express*, vol. 11, no. 9, pp. 147–153, 2014.
[17] D. C. Ludois, K. Hanson, and J. K. Reed, "Capacitive power transfer for slip ring replacement in wound field synchronous machines," in *Proc. IEEE Energy Convers. Congr. Exposition*, 2011, pp. 1664–1669.
[18] K. Jingook and F. Bien, "Electric field coupling technique of wireless power transfer for electric vehicles," in *Proc. IEEE TENCON Spring Conf.*, 2013, pp. 267–271.
[19] T. Ohira, "Via-wheel power transfer to vehicles in motion," in *Proc. IEEE Wireless Power Transfer*, 2013, pp. 242–246.
[20] F. Lu, H. Zhang, H. Hofmann, and C. Mi, "An inductive and capacitive combined wireless power transfer system with LC-compensated topology," *IEEE Trans. Power Electron.*, vol. 31, no. 12, pp. 8471–8482, Dec. 2016.
[21] K. Wang and S. Sanders, "Contactless USB—A capacitive power and bidirectional data transfer system," in *Proc. 29th Annu. IEEE Appl. Power Electron. Conf. Expo.*, 2014, pp. 1342–1347.
[22] D. Shmilovitz, S. Ozeri, and M. M. Ehsani, "A resonant LED driver with capacitive power transfer," in *Proc. 29th Annu. IEEE Appl. Power Electron. Conf. Expo.*, 2014, pp. 1384–1387.
[23] D. Jiejian and D. C. Ludois, "Biologically inspired coupling pixilation for position independence in capacitive power transfer surfaces," in *Proc. IEEE Appl. Power Electron. Conf. Expo.*, 2015, pp. 3276–3282.
[24] 3I Innovation Inc. (2015). Inductively powered LED lighting solutions. [Online]. Available: http://www.3iinnovation.com/
[25] m. Ltd. (2011). Wireless power transmission modules. [Online]. Available: http://www.murata.com/products/wireless_power/index.html
[26] X. Qu, W. Zhang, S. Wong, and C. Tse, "Design of a current-source-output inductive power transfer led lighting system," *IEEE J. Emerg. Select. Topics Power Electron.*, vol. 3, no. 1, pp. 306–314, Mar. 2015.
[27] B. Chen and Y. Lai, "New digital-controlled technique for battery charger with constant current and voltage control without current feedback," *IEEE Trans. Ind. Electron.*, vol. 59, no. 3, pp. 1545–1553, Mar. 2012.
[28] K. Zhou, P. Yao, and L. Cai, "Constant current vs. constant power control in AC resistance spot welding," *J. Mater. Process. Technol.*, vol. 223, pp. 299–304, Apr. 2015.
[29] L. Chao, A. P. Hu, B. Wang, and N. C. Nair, "A capacitively coupled contactless matrix charging platform with soft switched transformer control," *IEEE Trans. Ind. Electron.*, vol. 60, no. 1, pp. 249–260, Jan. 2013.
[30] M. P. Theodoridis, "Effective capacitive power transfer," *IEEE Trans. Power Electron.*, vol. 27, no. 12, pp. 4906–4913, Dec. 2012.
[31] J. Dai and D. Ludois, "Capacitive power transfer through a conformal bumper for electric vehicle charging," *IEEE J. Emerg. Select. Topics Power Electron.*, vol. 4, no. 3, pp. 1015–1025, Sep. 2015.
[32] S. K. Mishra, R. Adda, S. Sekhar, A. Joshi, and A. K. Rathore, "Power transfer using portable surfaces in capacitively coupled power transfer technology," *IET Power Electron.*, vol. 9, no. 5, pp. 997–1008, Apr. 2016.
[33] L. Chao, A. P. Hu, and N. C. Nair, "Coupling study of a rotary capacitive power transfer system," in *Proc. IEEE Int. Conf. Ind. Technol.*, 2009, pp. 1–6.
[34] A. Kumar, S. Pervaiz, C. Chang, S. Korhummel, Z. Popovic, and K. K. Afridi, "Investigation of power transfer density enhancement in large air-gap capacitive wireless power transfer systems," in *Proc. IEEE Wireless Power Transfer Conf.*, 2015, pp. 1664–1669.

Yu-Gang Su (M'09) received the B.E. and M.E. degrees in industry automation and the Ph.D. degree in control theory and control engineering from Chongqing University, Chongqing, China, in 1985, 1993, and 2004, respectively.

From 2008 to 2009, he was a Visiting Scholar with the University of Queensland, Brisbane, Australia. He is currently a Professor in the College of Automation, Chongqing University. His research interests include power electronics, control theory and applications, and wireless power transfer.

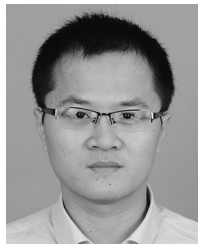

Shi-Yun Xie received the B.E. degree in the control of power eletronics from the College of Automation, Chongqing University, Chongqing, China, in 2010, where he is currently working toward the Ph.D. degree in control theory and control engineering.

His current research interests include the mixed-resonant topologies of capacitive power transfer systems and their control strategies, and wireless power transfer technologies.

Aiguo Patrick Hu (M'01–SM'07) received the B.E. and M.E. degrees in electrical engineering from Xi'an JiaoTong University, Xi'an, China, in 1985 and 1988, respectively, and the Ph.D. degree from the University of Auckland, Auckland, New Zealand, in 2001.

Before receiving the Ph.D. degree, he served as a Lecturer, a Director of the China Italy Cooperative Technical Training Center, Xian, and the General Manager of a technical development company. Funded by Asian2000 Foundation, he stayed in the National University of Singapore for a semester as an Exchange Postdoc Research Fellow. He holds 15 patents in wireless/contactless power transfer and microcomputer control technologies, published more than 200 peer reviewed journal and conference papers, authored a monograph on wireless inductive power transfer technology, and contributed 4 book chapters. He is currently in the Department of Electrical and Computer Engineering, University of Auckland, and also the Head of Research of PowerbyProxi Ltd. His research interests include wireless/contactless power transfer systems and application of power electronics in renewable energy systems.

Chun-Sen Tang (M'09) received the B.E. and Ph.D. degrees in wireless power transfer technology from the College of Automation, Chongqing University, Chongqing, China, in 2004 and 2009, respectively.

In 2008, he was a Research Fellow in the Department of Electrical and Computer Engineering, University of Auckland, Auckland, New Zealand. He joined the College of Automation, Chongqing University, Chongqing, China, in 2009 and is currently an Associate Professor. His current research interests include nonlinear modeling and analysis, intelligent control, and wireless power transfer.

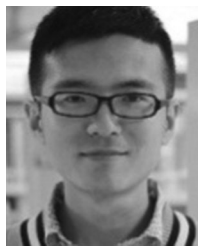

Wei Zhou received the B.E. degree in control of power eletronics from the College of Automation, Chongqing University, Chongqing, China, in 2013, where he is currently working toward the Ph.D. degree in control theory and control engineering.

He is currently a Visiting Scholar in the Department of Electrical and Computer Engineering, University of Auckland, Auckland, New Zealand. His current research interests include capacitive power transfer technology, wireless power, signal parallel transmissions, and control theory.

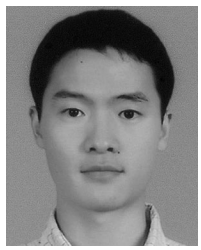

Liang Huang received the B.E. degree in electrical engineering from the Huazhong University of Science and Technology, Wuhan, China, in 2008, and the M.E. degree in mechatronic engineering from the Chongqing University, Chongqing, China, in 2011. He is currently working toward the Ph.D. degree in power electronics at the University of Auckland, Auckland, New Zealand.

His main research interests include power electronics, design and optimization of high-frequency inverters, wireless power transfer, and capacitive power transfer.